phys. stat. sol. (a) **205**, No. 7, 1713–1718 (2008) / **DOI** 10.1002/pssa.200723466

physica status solidi a
www.pss-a.com
applications and materials science

Intensity and temperature dependent characterization of eta solar cell

Robinson J. Musembi[*, 1], Marin Rusu[2], Julius M. Mwabora[1], Bernard O. Aduda[1], Konstantinos Fostiropoulos[2], and Martha Ch. Lux-Steiner[2]

[1] Department of Physics, School of Physical Sciences, University of Nairobi, P.O. Box 30197, 00100 Nairobi, Kenya
[2] Hahn-Meitner Institute, Glienicker Straße 100, 14109 Berlin, Germany

Received 27 September 2007, revised 2 April 2008, accepted 9 May 2008
Published online 19 June 2008

PACS 73.40.Ei, 73.40.Lq, 73.50.Gr, 73.50.Pz, 84.60.Jt

[*] Corresponding author: e-mail musembirj@uonbi.ac.ke, Phone: +254 20 444 75 52, Fax: +254 20 444 96 16

Temperature-dependent electrical characterization of a highly structured TiO_2/$In(OH)_xS_y$/$Pb(OH)_xS_y$/PEDOT:PSS eta solar cell has been carried out. The transport mechanism in this type of solar cell has been investigated. A schematic energy band diagram which explains the photoelectrical properties of the device has been proposed. The solar cell has been characterized in the temperature range 200–320 K at illumination intensities between 0.05 mW/cm^2 and 100 mW/cm^2. The diode ideality factor A under illumination has been found to vary between 1.2 and 1.6, whereas in the dark $6.9 \le A \le 10.1$. The device has been found to undergo a thermally activated recombination under illumination, while tunnelling enhanced recombination has been established to dominate the current in the dark. The solar cell efficiency shows a logarithmic dependence on illumination in the whole temperature range investigated, achieving its maximum at an illumination of ~45 mW/cm^2.

1 Introduction Design concepts for photovoltaic devices which are expected to yield high conversion efficiency using low cost production methods have been proposed over the years. The concept of an eta solar cell proposed a few years ago [1, 2] is a solar cell structure based on an extremely thin absorber (eta) material. The eta solar cell is similar to the dye-sensitized solar cell [3] but, instead of a monolayer of dye molecules, an eta material is sandwiched between two wide band gap n- and p-type materials. The photovoltaic effect of this cell structure is due to charge-carrier injection from the absorber layer.

In the literature, eta solar cells have been reported using various absorber materials, among them including CdTe [4], a-Si [5], $CuInS_2$ [6] and PbS [7, 8]. In earlier publications, Bayon et al. [7, 8] reported a highly structured eta solar cell with PbS as an absorber material, with TiO_2 and an organic material PEDOT:PSS (poly(3,4)ethylenedioxythiophene doped with polystyrene sulfonic acid) as n- and p-type wide band gap materials, respectively, and $In(OH)_xS_y$ as a buffer layer. However, some recent publications by Gavrilov et al. [9] and Oja et al. [10], which have employed for the preparation of $In(OH)_xS_y$ and $Pb(OH)_xS_y$ layers the SILAR (successive ion layer adsorption and reaction) technique rather than the chemical bath deposition used by Bayon et al. [7, 8], reported results on photovoltaic devices of the same structure, TiO_2/$In(OH)_xS_y$/$Pb(OH)_xS_y$/PEDOT:PSS, where the $In(OH)_xS_y$/$Pb(OH)_xS_y$ structure is called a charge-selective heterojunction [9]. Absorption properties are attributed to the $In(OH)_xS_y$ layer [10].

In this work, to clarify the role of component materials in the TiO_2/$In(OH)_xS_y$/$Pb(OH)_xS_y$/PEDOT:PSS heterostructure, devices with simplified architectures have been prepared by applying the layer elimination principle and analysis of the solar cells' photoelectrical properties. Moreover, we investigate the current transport mechanism, which has not yet been studied, despite the widely investigated properties of these types of devices [4, 6, 11, 12]. Therefore, in this work we report the temperature and light intensity dependent analysis of a highly structured TiO_2/$In(OH)_xS_y$/$Pb(OH)_xS_y$/PEDOT:PSS eta solar cell.

2 Experimental procedure The solar cells were processed by the following procedure: the substrate used was a 15 Ω/□ sheet resistance SnO_2:F glass from For-

schungszentrum Jülich. A 2 μm thick titanium dioxide, TiO_2, film was coated on the SnO_2:F glass by the sol–gel technique at SgLux GmbH company. On top of TiO_2, an 80 nm thick indium hydroxyl sulphide, $In(OH)_xS_y$, and a 10 nm thick lead hydroxyl sulphide, $Pb(OH)_xS_y$ thin film were successively deposited by chemical bath deposition using the following precursors: for $In(OH)_xS_y$ an aqueous solution containing $InCl_3$ (0.025 M), thioacetamide (0.1 M) and HCl (0.005 M) was deposited at 70 °C for 30 min and repeated three times following the procedure described by Bayon et al. [7, 8, 13]. Also, $Pb(OH)_xS_y$ was deposited from an aqueous solution containing $Pb(CH_3OOH)_2$ (0.05 M), NaOH (0.2 M), triethanolamine (0.05 M) and thiourea (0.05 M) at 40 °C for 10 min using a procedure as reported elsewhere [7, 8]. The last layer, an undiluted PEDOT:PSS polymer material type Baytron PH from Bayer GmbH, was then spin coated on top of $Pb(OH)_xS_y$. The front and back contacts of the solar cells were coated using a special mask which gave solar cells of 0.126 cm^2 areas. The structure of the complete solar cell was SnO_2:F/TiO_2/$In(OH)_xS_y$/$Pb(OH)_xS_y$/PEDOT:PSS/Au.

Measurement of the temperature-dependent current–voltage characteristics ($JV–T$) was performed in an evacuated nitrogen-cooled cryostat using a Keithley 2400 series current voltage source meter. A halogen lamp (General Electric™, 120 V, 300 W, type L268) calibrated to 100 mW/cm^2 (calibration: 100 mW/cm^2 = 1 sun AM1.5) was used as a light source and a set of neutral density filters were used for adjusting the light intensity. The experiments were performed as follows: the temperature was first lowered to T = 200 K, and then $J–V$ characteristics were taken starting with the measurement in the dark, followed by 12 successive measurements under illumination. The light intensity was decreased from 100 mW/cm^2 to 0.05 mW/cm^2 by using neutral density filters. The same procedure was applied for each temperature measurement up to 320 K, the temperature being consecutively changed in steps of 10 K.

3 Device architectures and the role of component materials Table 1 presents the photovoltaic parameters of an eta solar cell with complete SnO_2:F/TiO_2/$In(OH)_xS_y$/$Pb(OH)_xS_y$/PEDOT:PSS/Au structure as well as those of the devices with simplified structures. The devices with simplified structures were prepared for clarifying the role of the individual layers. An efficiency of about 0.8% was achieved in the full-structure device A. Even higher efficiency was achieved in the device B which does not contain the PEDOT layer. As is seen, the same tendency to show slightly higher efficiencies is characteristic also for the devices of type D when compared with the devices of type C, which do not contain the TiO_2 layer. Slightly higher efficiencies in samples which do not contain the PEDOT layer are achieved mainly because of higher fill factors. The recorded short-circuit currents are comparable (compare samples C and D) or slightly lower (compare samples A and B). As will be shown in Section 5, the $Pb(OH)_xS_y$/PEDOT interface is not a junction that may separate charge carriers under illumination. As the PEDOT is a hole conductor and its valence-band maximum (E_v) in the present structure is well adjusted to E_v of the $Pb(OH)_xS_y$, the lowering of J_{sc} in sample B can be attributed to the effect of the 'bulk' resistance of this material, e.g. effects caused by variations in the PEDOT layer thickness, as well as complete coverage of the $Pb(OH)_xS_y$ surface. Another effect observed is that both A and C type devices with PEDOT layers show much higher stability than the devices without this layer. Therefore, it can be concluded that the PEDOT layer possesses, besides other favourable electrical purposes, a protective layer function against diffusion of the Au atoms from the rear contact through the complete structure and thus shunting the device.

For clarifying the role of TiO_2, samples A and C are compared. In both samples similar open-circuit voltages and fill factors are observed, while the short-circuit current of the device C is about 35% lower than that of the device A. Thus, presence of the TiO_2 layer at the SnO_2/$In(OH)_xS_y$ interface reduces the recombination rate at the front contact. At the same time, higher short-circuit currents are recorded in sample A also because of the increased area of the device due to the use of highly structured TiO_2 thin films.

The role of $In(OH)_xS_y$ becomes clear from the comparison of the devices A and E. The device E, which is prepared without the $In(OH)_xS_y$ layer, shows very low photovoltaic parameters. Moreover, the $J–V$ characteristics of the SnO_2:F/TiO_2/$Pb(OH)_xS_y$/PEDOT:PSS/Au structures (not shown) show high inverse tunnelling currents. Therefore, it is not surprising that in the regime of a solar cell these structures show a V_{oc} = 14 mV. At the same time, the device A with $In(OH)_xS_y$ and $Pb(OH)_xS_y$ layers shows a

Table 1 Photovoltaic parameters of a complete SnO_2:F/TiO_2/$In(OH)_xS_y$/$Pb(OH)_xS_y$/PEDOT:PSS/Au eta solar cell and of the devices with simplified structures.

solar cell	device structure	J_{sc} (mA/cm^2)	V_{oc} (mV)	FF	eff. (%)
A	SnO_2:F/TiO_2/$In(OH)_xS_y$/$Pb(OH)_xS_y$/PEDOT:PSS/Au	7.40	281	0.40	0.83
B	SnO_2:F/TiO_2/$In(OH)_xS_y$/$Pb(OH)_xS_y$/Au	6.16	344	0.44	0.94
C	SnO_2:F/$In(OH)_xS_y$/$Pb(OH)_xS_y$/PEDOT:PSS/Au	4.95	314	0.40	0.61
D	SnO_2:F/$In(OH)_xS_y$/$Pb(OH)_xS_y$/Au	5.33	297	0.41	0.65
E	SnO_2:F/TiO_2/$Pb(OH)_xS_y$/PEDOT:PSS/Au	1.8×10^{-3}	14	0.25	0.01

reasonable V_{oc} of about 280 mV and an efficiency of 0.83%. Therefore, we conclude that the interface responsible for the separation of the charge carriers in the eta solar cells presented is $In(OH)_xS_y/Pb(OH)_xS_y$.

4 Transport mechanism evaluation approach

We apply for analysis of the dark and illuminated $JV-T$ curves the one-diode model developed for polycrystalline heterojunction thin film solar cells [14, 15]. According to this model, the forward current density J of the heterojunction is described by

$$J = J_0 \exp\left(\frac{qV}{AkT}\right) = J_{00} \exp\left(\frac{-E_a}{AkT}\right) \exp\left(\frac{qV}{AkT}\right), \quad (1)$$

where A and J_0 are the ideality factor and saturation current density of the diode, respectively, kT/q is the thermal voltage, J_{00} is the weakly temperature dependent prefactor and E_a defines the activation energy of recombination. According to Eq. (1), the open-circuit voltage V_{oc} is

$$V_{oc} \approx \frac{AkT}{q} \ln\left(\frac{J_{sc}}{J_0}\right) = \frac{E_a}{q} - \frac{AkT}{q} \ln\left(\frac{J_{00}}{J_{sc}}\right), \quad (2)$$

where J_{sc} is the short-circuit current density. Equation (2) relates the open-circuit voltage to the activation energy. Hence, a plot of V_{oc} versus T should yield a straight line, an extrapolation to $T = 0$ K giving the activation energy E_a (Eq. (2)). When the tunnelling process is significant, Eq. (2) can be reorganized to give

$$A \ln J_0 = -\frac{E_a}{kT} + A \ln J_{00} . \quad (3)$$

As mentioned above, E_a can be extracted even more precisely from a plot of the corrected saturation current density $A \ln J_0$ versus the inverse temperature $1/T$, which yields a straight line with a slope corresponding to the activation energy E_a. The value of E_a indicates either bulk recombination when $E_a = E_g$ (E_g is the band-gap energy), or interface recombination for $E_a < E_g$.

5 Results and discussion

5.1 Transport mechanism As shown in Section 3, the devices of complete structure $SnO_2:F/TiO_2/In(OH)_xS_y/Pb(OH)_xS_y/PEDOT:PSS/Au$ with the PEDOT layer show good stability, therefore being suitable for the analysis of the transport mechanism. The investigation of the temperature-dependent current–voltage characteristics was performed for a solar cell which showed, under AM1.5 conditions (25 °C, 100 mW/cm^2), the following parameters: $V_{oc} = 0.249$ V, $J_{sc} = 9.24$ mA/cm^2, a fill factor FF = 0.34 and an efficiency of 0.78%.

The data obtained from the dark and illuminated $JV-T$ curves was plotted as shown in Fig. 1. Significant differences are observed between the dark and illuminated $JV-T$ and $J_{sc}V_{oc}-T$ curves. However, the curves in all the cases can be fitted to the one-diode model described in Section 3. It is worth mentioning that in the temperature range 200–300 K the J_{sc} versus V_{oc} plots exhibit an exponential dependence over two orders of magnitude. This fact makes these dependences suitable for fitting with reliable results. Thus, the diode ideality factor A and the saturation current J_0 as a function of temperature and illumination were determined by fitting the dark $JV-T$ and illuminated $J_{sc}V_{oc}-T$ curves to Eqs. (1) and (2), respectively. The temperature dependence of the diode ideality factor A is given in Fig. 2.

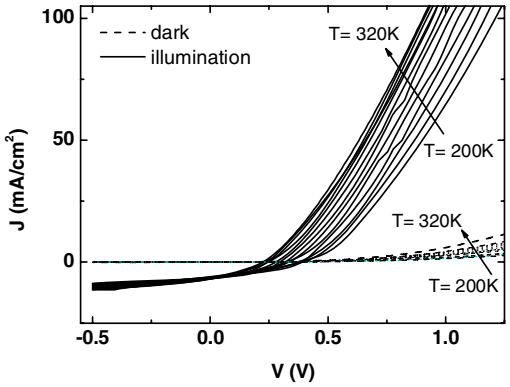

Figure 1 Current–voltage characterization in the dark and under illumination at different temperatures in the range 200–320 K.

The ideality factor of the solar cell under illumination was given by $1.2 \le A \le 1.6$, while in the dark $6.9 \le A \le 10.1$. The fluctuations of the diode quality factors in the latter case are attributed to the charge–discharge effects of the deep levels present in $In(OH)_xS_y$ [10]. This temperature behaviour of A indicates that in the dark the recombination is dominated by tunnelling, while under illumination the charge-carrier recombination is thermally activated. Moreover, continuous increase of A under illumination from ~1.0 K at 320 K to 1.6 K at 200 K shows that recombination occurs through exponentially distributed energy recombination levels [16]. Thus, under illumination and high temperatures recombination occurs through shallow levels ($A \sim 1$), while at low temperatures

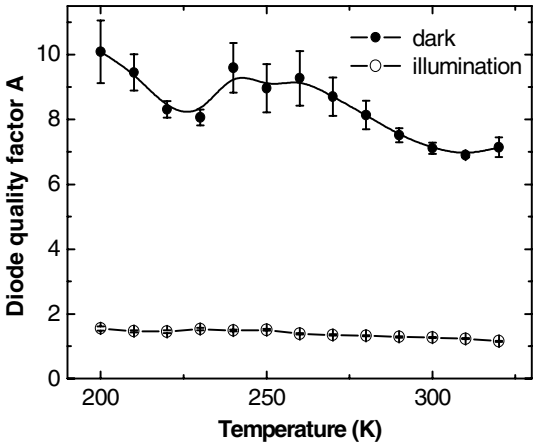

Figure 2 Temperature dependence of the diode quality factor as extracted from dark JV curves and J_{sc} versus V_{oc} as extracted from Fig. 1.

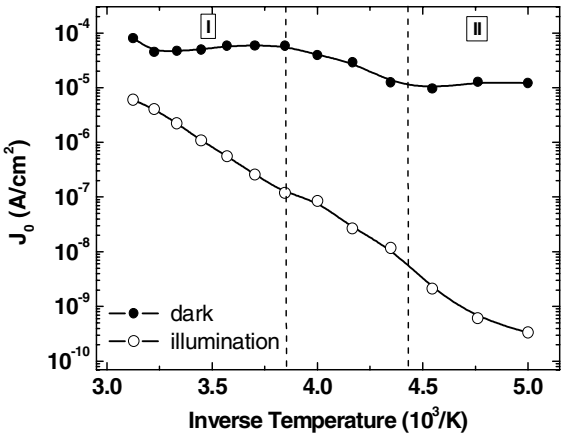

Figure 3 Temperature-dependent reverse saturation current density as a function of inverse temperature as extracted from dark and illuminated $JV-T$ characteristics in Fig. 1.

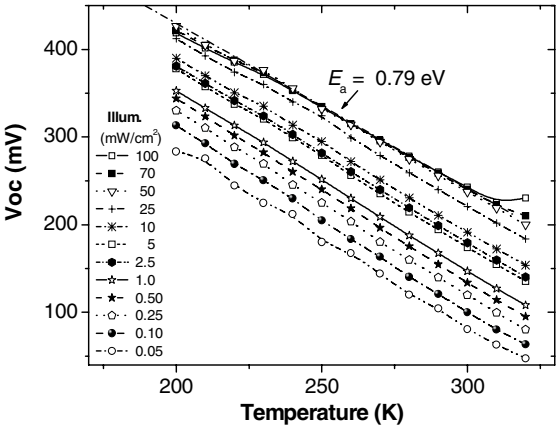

Figure 5 Efficiency of the eta solar cell as a function of illumination intensity at different temperatures.

deep levels are involved in the recombination. The findings of tunnelling dominated recombination in the dark and thermally dominated recombination under illumination are supported by the temperature behaviour of saturation current density J_0 as a function of temperature as shown in Fig. 3. The $J_0 = f(1/T)$ curve in Fig. 3 (in the dark) shows two regions I and II where saturation current densities are independent of the inverse temperature, confirming the tunnelling assisted recombination mechanism. Under illumination a linear decrease of J_0 with increasing $1/T$ is observed in the entire temperature region investigated (Fig. 3), which confirms that a thermally activated mechanism dominates the recombination.

The modified Arrhenius plot $A \ln(J_0)$ as a function of inverse temperature $1/T$, as in Fig. 4, gives the value of the activation energy $E_a = 0.92$ eV. The activation energy of recombination was also determined from $V_{oc} = f(T)$ plots in Fig. 5. Plotting V_{oc} as a function of temperature T and assuming that A, J_{sc} and J_{oo} are independent of temperature in Eq. (2), a linear extrapolation to $T = 0$ K gives an activation energy $E_a = 0.79$ eV.

As is observed, both methods of determining the activation energy of recombination give values that are close to the band gap $E_a = 0.83$ eV of the chemical bath deposited $Pb(OH)_xS_y$, as reported elsewhere [7]. Thus, from this analysis it follows that $E_a \approx E_g$, indicating recombination in the $Pb(OH)_xS_y$ layer and giving a hint that the absorber band gap could be engineered for further widening.

The observed findings are supported by the schematic energy band diagram proposed in Fig. 6, which is based on data in Table 2. Thus, strong tunnelling effects in the dark are related to the presence of a cliff in the conduction band at the $TiO_2/In(OH)_xS_y$ interface, of a spike in the $In(OH)_xS_y$ conduction band and of the deep recombination levels exponentially distributed in energy in the $In(OH)_xS_y$ band gap [10]. The electrons injected from the $SnO_2:F/TiO_2$ front electrode recombine through deep levels in $In(OH)_xS_y$ with the holes from the $Pb(OH)_xS_y$ valence band.

Under illumination the $In(OH)_xS_y$ bands become flat and the deep levels filled. Therefore, in an illuminated device the recombination path shifts from $In(OH)_xS_y$ into the $Pb(OH)_xS_y$ layer.

It has to be mentioned that the $Pb(OH)_xS_y$ layer, which shows absorption properties in surface photovoltage measurements [10], does not contribute to the quantum efficiency of the devices, which extends just between 350 nm and 800 nm (not shown). However, this is not surprising

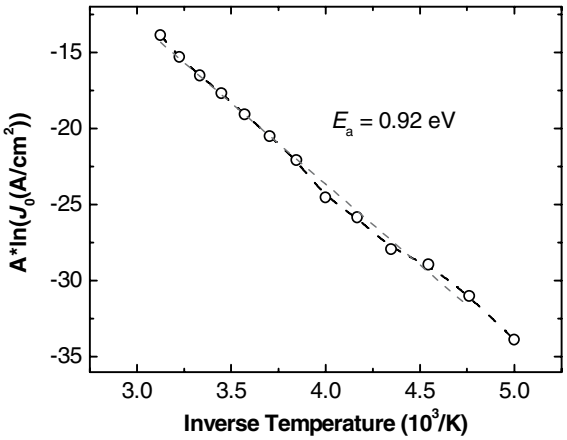

Figure 4 Arrhenius plot of the saturation current density J_0 corrected by diode ideality factor A with the data extracted from illuminated characteristics.

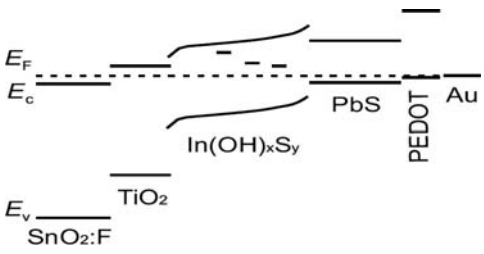

Figure 6 Proposed band diagram for the eta solar cell of the structure $SnO_2:F/TiO_2/In(OH)_xS_y/Pb(OH)_xS_y$/PEDOT:PSS.

Table 2 Electronic parameters of the SnO_2:F/TiO_2/In$(OH)_xS_y$/Pb$(OH)_xS_y$/PEDOT:PSS/Au eta solar cell component materials, where Φ denotes the work function, χ the electron affinity and E_g the band gap.

material	Φ (eV)	χ (eV)	E_g (eV)
SnO_2:F	4.5 [17]	5.0 [17]	3.8 [17]
TiO_2	4.5 [17]	4.3 [17]	3.2 [17]
In$(OH)_xS_y$	4.7 [10]	3.7*	2.4 [7]
Pb$(OH)_xS_y$	5.0 [18]	4.5** [19]	0.85 [7]
PEDOT:PSS	5.2 [20]	3.2 [21]	2.0 [21]
Au	5.1 [22]		

* approximated value; ** recalculated value considering as reference for the energy scale the vacuum level instead of normal hydrogen electrode.

when considering the band diagram in Fig. 6: the charge carriers generated under illumination in the Pb$(OH)_xS_y$ layer will effectively recombine at the In $(OH)_xS_y$/Pb$(OH)_xS_y$ interface, since large barriers for charges are present in both valence and conduction bands at this interface. The greatest contribution to the device's quantum efficiency is observed from the In $(OH)_xS_y$ layer showing its absorber role in the given system. The role of the Pb$(OH)_xS_y$ as absorber in the present SnO_2:F/TiO_2/In$(OH)_xS_y$/Pb$(OH)_xS_y$/PEDOT:PSS/Au heterostructure is minimized because of a specific band arrangement at the In$(OH)_xS_y$/Pb$(OH)_xS_y$ interface.

5.2 Illumination characteristics The illumination dependence of the open-circuit voltage at different temperatures is presented in Fig. 7. For all investigated temperatures, the open-circuit curves exhibit a logarithmic correlation with varying illumination intensity from 0.05 mW/cm^2 to 100 mW/cm^2. The short-circuit current density shows a linear dependence on illumination, being weakly dependent on temperature (not shown).

The fill factor is barely dependent on illumination and temperature, its value varying between 0.30 and 0.36 (not shown). As a result, the efficiency of the eta solar cell was found to have a logarithmic correlation with illumination intensity, as shown in Fig. 8.

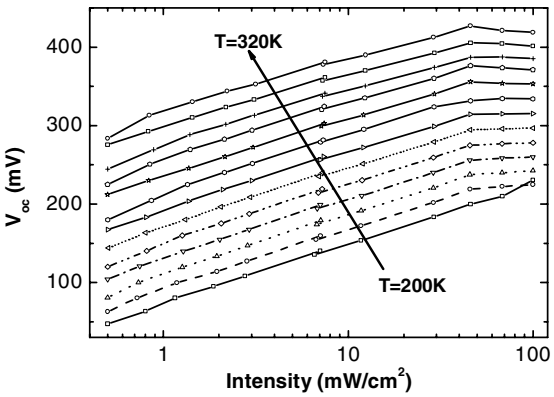

Figure 7 Open-circuit voltage V_{oc} of the eta solar cell as a function of illumination intensity at different temperatures.

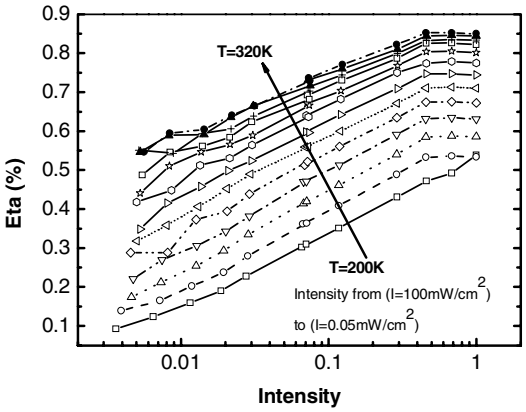

Figure 8 Efficiency of the eta solar cell as a function of illumination intensity at different temperatures.

A maximum efficiency of the solar cell was achieved at an illumination of ~45 mW/cm^2. Temperature has a strong impact on the device's conversion efficiency. The efficiency changes from 0.5% to 0.8% when the temperature increases from 200 K to 300 K.

6 Conclusion The role of component materials of the SnO_2:F/TiO_2/In$(OH)_xS_y$/Pb$(OH)_xS_y$/PEDOT:PSS/Au eta solar cell has been clarified, the transport mechanism in these devices has been investigated and an energetic band diagram that explains the observed experimental features has been proposed.

The Pb$(OH)_xS_y$ action as absorber layer is minimized because of recombination processes at the In$(OH)_xS_y$/Pb$(OH)_xS_y$ interface. Nevertheless, the latter interface separates the charges generated in illuminated devices.

The solar cell has been found to undergo bulk thermally activated recombination under illumination. A different recombination mechanism is observed in the dark. In this case, the solar cell has been observed to undergo tunnelling enhanced recombination.

The solar cell has been found to have a logarithmic correlation of the efficiency and the open-circuit voltage as a function of illumination intensity, while the fill factor is independent of the illumination intensity and temperature. The short-circuit current of the eta device shows a linear dependence on the illumination intensity and a weak temperature dependence.

References

[1] S. Siebentritt, K. Ernst, C.-H. Fischer, R. Koenenkamp, and M. Ch. Lux-Steiner, Proc. 14th Eur. Photovoltaic Solar Energy Conf. Exhib., Barcelona, Spain, 1997, p. 1823.
[2] I. Kaiser, K. Ernst, C.-H. Fischer, R. Koenenkamp, C. Rost, I. Sieber, and M. Ch. Lux-Steiner, Sol. Energy Mater. Sol. Cells **67**, 89 (2001).
[3] B. O'Regan and M. Gratzel, Nature **353**, 8720 (1990).
[4] K. Ernst, R. Engelhardt, K. Ellmer, C. Kelch, H. J. Muffler, M. Ch. Lux-Steiner, and R. Koenenkamp, Thin Solid Films **387**, 26 (2001).

[5] A. Wahi and R. Koenenkamp, Proc. 11th Photovoltaic Solar Energy Conf., Montreux, Switzerland, 1992, p. 714.
[6] I. Kaiser, K. Ernst, C.-H. Fischer, C. Rost, I. Sieber, M. Ch. Lux-Steiner, and R. Koenekamp, Sol. Energy Mater. Sol. Cells **67**, 89 (2001).
[7] R. Bayon, R. Musembi, A. Belaidi, M. Bar, T. Guminskaya, M. Ch. Lux-Steiner, and T. Dittrich, Sol. Energy Mater. Sol. Cells **89**, 13 (2005).
[8] R. Bayon, R. Musembi, A. Belaidi, M. Bar, T. Guminskaya, C.-H. Fischer, M. Ch. Lux-Steiner, and T. Dittrich, C.R. Chim. **9**, 730 (2006).
[9] S. Gavrilov, I. Oja, B. Lim, A. Belaidi, W. Bohne, E. Strub, J. Rohrich, M. Ch. Lux-Steiner, and T. Dittrich, phys. stat. sol. (a) **203**(5), 1024 (2006).
[10] I. Oja, A. Belaidi, L. Dloczick, M. Ch. Lux-Steiner, and T. Dittrich, Semicond. Sci. Technol. **21**, 520 (2006).
[11] F. Lenzmann, B. O'Regan, J. Wienke, C. Huismann, L. Reijnen, and A. Goossens, Physica E **14**, 233 (2002).
[12] C. L. Clement, R. T. Zaera, M. A. Ryan, A. Katty, and G. Hodes, Adv. Mater. **17**, 1512 (2005).
[13] R. Bayon, C. Guillen, M. A. Martinez, M. T. Guitierrez, and J. Herrero, J. Electrochem. Soc. **145**, 2775 (1998).
[14] V. Nadenau, U. Rau, and A. Jasenek, J. Appl. Phys. **87**, 584 (2000).
[15] M. Rusu, W. Eisele, R. Wurz, A. Ennaoui, M. Ch. Lux-Steiner, T. P. Niesen, and F. Karg, J. Phys. Chem. Solids **64**, 2037 (2003).
[16] T. Walter, R. Herberholz, and H. W. Schock, Solid State Phenom. **51/52**, 309 (1996).
[17] M. Grätzel, Nature **414**, 339 (2001).
[18] R. Musembi et al., unpublished.
[19] R. Vogel, P. Hoyer, and H. Weller, J. Phys. Chem. **98**, 3183 (1994).
[20] T. M. Brown, J. S. Kim, R. H. Friend, F. Cacialli, R. Daik, and W. J. Feast, Appl. Phys. Lett. **75**, 1679 (1999).
[21] M. J. Song, K.-J. Kim, and D. Y. Kim, Sol. Energy Mater. Sol. Cells **85**, 31 (2005).
[22] D. E. Eastman, Phys. Rev. B **2**, 1 (1970).

